Two-color two-photon excited fluorescence of indole: Determination of wavelength-dependent molecular parameters

Sebastian Herbrich, Tawfik Al-Hadhuri, Karl-Heinz Gericke, Peter S. Shternin, Andrey G. Smolin, and Oleg S. Vasyutinskii

Citation: The Journal of Chemical Physics **142**, 024310 (2015); doi: 10.1063/1.4905140
View online: http://dx.doi.org/10.1063/1.4905140
View Table of Contents: http://scitation.aip.org/content/aip/journal/jcp/142/2?ver=pdfcov
Published by the AIP Publishing

Two-color two-photon excited fluorescence of indole: Determination of wavelength-dependent molecular parameters

Sebastian Herbrich,[1] Tawfik Al-Hadhuri,[1] Karl-Heinz Gericke,[1,a)] Peter S. Shternin,[2,3,b)] Andrey G. Smolin,[2] and Oleg S. Vasyutinskii[2,3,c)]
[1]*Institut für Physikalische und Theoretische Chemie, TU Braunschweig, Hans-Sommer-Straße 10, 38106 Braunschweig, Germany*
[2]*Ioffe Institute, Politekhnicheskaya 26, 194021 St. Petersburg, Russia*
[3]*St. Petersburg Polytechnic University, Politekhnicheskaya 29, St. Petersburg 195251, Russia*

(Received 13 October 2014; accepted 16 December 2014; published online 12 January 2015)

We present a detailed study of two-color two-photon excited fluorescence in indole dissolved in propylene glycol. Femtosecond excitation pulses at effective wavelengths from 268 to 293.33 nm were used to populate the two lowest indole excited states ^1L_a and ^1L_b and polarized fluorescence was then detected. All seven molecular parameters and the two-photon polarization ratio Ω containing information on two-photon absorption dynamics, molecular lifetime τ_f, and rotation correlation time τ_{rot} have been determined from experiment and analyzed as a function of the excitation wavelength. The analysis of the experimental data has shown that ^1L_b–^1L_a inversion occurred under the conditions of our experiment. The two-photon absorption predominantly populated the ^1L_a state at all excitation wavelengths but in the 287–289 nm area which contained an absorption hump of the ^1L_b state 0-0 origin. The components of the two-photon excitation tensor **S** were analyzed giving important information on the principal tensor axes and absorption symmetry. The results obtained are in a good agreement with the results reported by other groups. The lifetime τ_f and the rotation correlation time τ_{rot} showed no explicit dependence on the effective excitation wavelength. Their calculated weighted average values were found to be $\tau_f = 3.83 \pm 0.14$ ns and $\tau_{rot} = 0.74 \pm 0.06$ ns. © *2015 AIP Publishing LLC.* [http://dx.doi.org/10.1063/1.4905140]

I. INTRODUCTION

Two-photon excitation spectroscopy is now a well-established technique for assigning molecular excited-state energy levels and wave functions.[1] In biological studies, it has undeniable advantages in comparison with one-photon techniques due to its non-invasive character and possibility of precise spatial focusing. One of the most informative multi-photon methods deals with the investigation of two-photon excited fluorescence (TPEF) spectra and polarization.[2,3] While most of the TPEF studies relied on the two-photon excitation with identical photons, the most general TPEF experiments employ a two-color two-photon (2C2P) excitation scheme.[4–9] In his seminal paper,[10] McClain has pointed out that for any experimental geometry the fluorescence polarization can be described by a linear combination of a number of molecular parameters which depend only on the intermolecular properties and excited state dynamics. As shown by McClain,[11] if the molecular excited state is not degenerate, the total number of molecular parameters is seven. Different definitions of the molecular parameters were suggested by McClain,[10] Metz *et al.*,[12] Gaisenok,[13] Wan and Johnson,[14] and Shternin, Gericke, and Vasyutinskii.[15]

The use of femtosecond laser pulses in TPEF experiments makes it possible to track the evolution of the fluorescence from the anisotropic ensembles of excited molecules in the real time domain with high temporal resolution.[8,16] The Braunschweig group[8,9,17,18] has recently used the femtosecond 2C2P excitation scheme for detailed investigation of important UV fluorophores: *p*-terphenyl (PTP)[17] and 2-methyl-5-*t*-butyl-*p*-quaterphenyl (DMQ).[18] The complete set of molecular parameters has been determined from experiment in those studies which met the conditions of the complete polarization experiment.

This paper presents the study of indole at seven effective excitation wavelengths in the spectral region 268–294 nm using the theory and experimental setup developed in our previous studies.[15,17,18] Indole (C_8H_7N), the chromophore of the amino acid tryptophan, attracted much attention of theoretical and experimental groups all over the world during latest decades as an important fluorescent marker responsible for most of the UV absorption in proteins.[19] The indole excitation properties and fluorescence behavior in various media are governed by two close-lying lowest excited states conventionally noted as ^1L_a and ^1L_b.[20] These states belong to the same A' symmetry of the molecular C_s point group and can be only designated by their different spectroscopic properties. In particular, it was found that the transition to the ^1L_b state is structured, naphthalene-like with a prominent 0-0 band and short Franck-Condon progressions, while the stronger transition to the ^1L_a state is broader and shows less features,

a)Electronic mail: k.Gericke@tu-bs.de
b)Electronic mail: pshternin@gmail.com
c)Electronic mail: osv@pms.ioffe.ru

with the absorption maximum shifted typically 3000 cm^{-1} to higher energy relative to the ^1L_b 0-0 band.

The transition dipole moments from the ground state to the ^1L_a and ^1L_b states are almost perpendicular to each other, with the ^1L_a transition dipole directed about −45° from the long axis in indole.[21] In the gas phase, the ^1L_b state is lower in energy with the origin located at 4.37 eV.[22] The origin of the ^1L_a state in the gas phase is not yet exactly known; however, several studies indicate that it is located at about 1400 cm^{-1} above the ^1L_b origin,[23–25] 4.54 eV above the ground state. The energy shift of the ^1L_a state in polar solvents is much larger than that of the ^1L_b state because the ^1L_a dipole moment is about three times larger than the ^1L_b one.[26,27] As known,[23,28] in some polar solvents, the energy shift difference can even cause inversion of the states.

In this paper, the TPEF polarization technique was used for obtaining detailed photodynamic information on indole dissolved in propylene glycol. Using the experimental procedure and method of the experimental data analysis developed in our previous papers,[15,17] we experimentally determined and analyzed seven molecular parameters $M_K(R,R')$, the two-photon polarization ratio Ω, and the components of the two-photon excitation tensor $S_{R\gamma}$ containing important information on the principal tensor axes and the anisotropy of indole two-photon absorptivity. The results obtained are in perfect agreement with the analysis by Callis[29] who theoretically reconstructed the two-photon excitation tensors for ^1L_a and ^1L_b states. It was also shown that the two-photon absorption predominantly populated the ^1L_a state at all excitation wavelengths except the 287–289 nm area where the absorption to the ^1L_b 0-0 origin was observed. The obtained spectral dependence of the two-photon polarization ratio Ω manifests that ^1L_b–^1L_a state inversion occurs under the conditions of our experiment, which is in agreement with the quantitative criterion of Catalán and Diáz.[30] The temporal evolution of indole excited states has also been studied by determination of the lifetime τ_f and the rotation correlation time τ_{rot} which did not show any explicit dependence on the effective excitation wavelength.

II. EXPERIMENTAL ARRANGEMENT

The experimental setup based on the 2C2P excitation scheme and the procedure of processing the experimental data used in the present study are described in detail elsewhere.[17,18] The scheme of the experimental setup is sketched in Fig. 1. Briefly, one of the excitation laser beams was the fundamental output of a Ti:sapphire femtosecond oscillator and the second excitation beam was the second harmonic of the oscillator output. The beams were separated by a dichroic mirror, the polarization of each beam was controlled separately by crystal polarizers and λ/2- and λ/4-waveplates. The beams propagated in opposite directions and both were focused onto the center of the absorption cuvette. Note, that Denicke *et al.*[17] used the beams propagating in the same direction. Tuning the oscillator output frequency in the 700–1000 nm spectral range provided two-photon excitation of indole at an effective one-photon wavelength range of 240–330 nm. The fluorescence was collected along the perpendicular direction

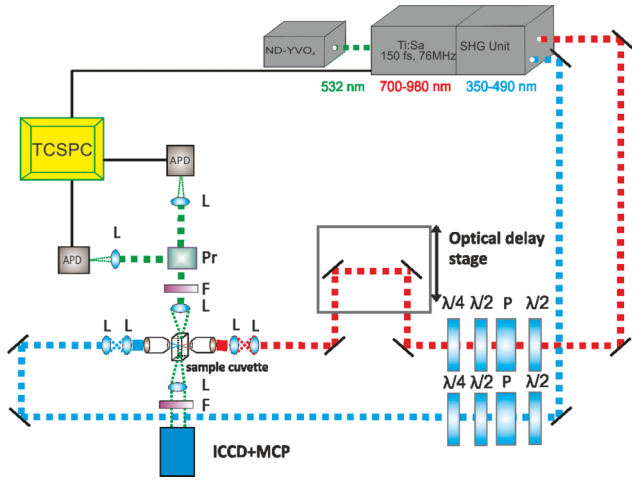

FIG. 1. The sketch of the experimental setup. P's are polarizers, L's are lenses, F's are filters, and Pr is a prism.

to the excitation beams. The time-dependent fluorescence polarization was monitored by a polarization prism and two fast photodetectors.

The experiments were performed at seven different excitation wavelengths listed in the first column in Table I which relate to the low-wavelength area of the two-photon excitation spectrum of indole dissolved in propylene glycol. Indole solutions were prepared yielding a concentration of 25 mM. Indole (≥99 percent, Sigma-Aldrich) and propylene glycol (≥99.5 percent, Sigma-Aldrich) were used without further purification. The fluorescence photons were detected in the photon counting regime using a time correlated single photon counting system.

Several different polarizations of the two excitation photons and the fluorescence photon were combined to determine from experiment seven time-dependent molecular parameters containing important information on the two-photon excitation step and the subsequent evolution of the molecular excited state. We used four different polarizations for each of the two excitation photons: vertical V (along Z axis), horizontal H (along Y axis), right-hand circularly polarized (R), and left-hand circularly polarized (L). These were combined with two orthogonal linear polarizations (X and Y) of the fluorescence photon. These geometries allowed

TABLE I. Intensities for different effective excitation geometries and wavelengths λ normalized to the values of I_{HH}. Mean values and standard deviations are estimated from three independent measurements for each wavelength. Δ is the normalized control sum, see text for details.

λ, nm	I_{VH}	$\Omega = I_{RL}$	I_{RR}	Δ
268	0.39 ± 0.02	0.73 ± 0.01	0.59 ± 0.01	0.06 ± 0.06
280	0.33 ± 0.02	0.71 ± 0.05	0.64 ± 0.05	−0.01 ± 0.08
286	0.40 ± 0.01	0.73 ± 0.02	0.67 ± 0.03	0.00 ± 0.04
287	0.42 ± 0.02	0.86 ± 0.03	0.60 ± 0.03	−0.04 ± 0.08
288	0.43 ± 0.04	0.85 ± 0.02	0.59 ± 0.02	−0.01 ± 0.01
289	0.41 ± 0.02	0.88 ± 0.03	0.58 ± 0.04	−0.04 ± 0.08
293.33	0.36 ± 0.02	0.70 ± 0.03	0.66 ± 0.04	0.00 ± 0.04

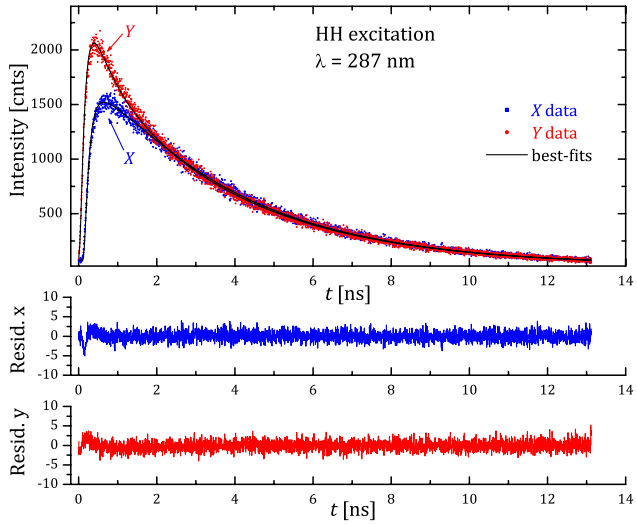

FIG. 2. Top panel: Example of experimental data obtained at effective excitation wavelength of 287 nm and HH combination of the excitation beams polarizations. The data counts in X and Y detection channels are indicated by squares and circles, respectively. Solid lines show respective two-exponential best-fit time-dependencies, see text for more details. Middle panel: Fit residuals for X channel. Bottom panel: Fit residuals for Y channel.

to obtain eight time-dependent experimental signals and determine the molecular parameters.[17]

An example of the experimental signal obtained at 287 nm is shown in the top panel of Fig. 2 where red and blue dots represent X and Y fluorescence polarizations for the (HH) excitation geometry. The excitation pulse duration was about 0.1 ps and the excitation occurred at $t = 0$. As can be seen from Fig. 2, the X-Y anisotropy is significant for times $t \le 2$ ps after excitation, but is negligible at longer times. Therefore, the polarized fluorescence signal contains isotropic and anisotropic parts with different time-dependencies. The signals in the X and Y detection channels can be written as[17]

$$I_{lX} = I_l(t)[1 + 2r_l(t)], \quad (1)$$

$$I_{lY} = I_l(t)[1 - r_l(t)], \quad (2)$$

where the index l stands for RR or RL, $r_l(t)$ is the anisotropy, and $I_l(t)$ is the isotropic intensity. In case of HH excitation geometry, the indices X and Y should be interchanged. Note that for the VH excitation geometry, the fluorescence signals related to two orthogonal polarizations do not follow the linear relations in Eqs. (1) and (2) and separate anisotropies $r_{VHX}(t)$ and r_{VHY} for X and Y channels, respectively, were introduced, see Ref. 17 for more details.

The intensities $I_l(t)$ in Eqs. (1) and (2) decay exponentially with the excited state lifetime τ_f and the anisotropy $r_l(t)$ evolves in time due to the rotational diffusion. In general, there can be several rotational diffusion times; however, for the prolate ellipsoids like indole, only one rotational correlation time τ_{rot} can be measured in the TPEF experiments.[31] Only in some cases, two rotational correlation times can be resolved in oblate molecules.[16] In this study, a two-exponential decay law was used for analysis of the polarized fluorescence signals in Eqs. (1) and (2), and it was found that it perfectly fitted the experimental data.

III. DATA PROCESSING

The experimental data were fitted following the procedure described in detail by Denicke *et al.*[17] giving the values of the fluorescence intensities and anisotropies at zero time, $t = 0$, and the decay and correlation times τ_f and τ_{rot}. The expressions in Eqs. (1) and (2) were convoluted with the instrumental response function (IRF), which was measured separately. Also, sensitivity difference between the X and Y detection channels was accounted for by introducing a scaling factor G. The global fit for all eight experimental geometries was performed using τ_f, τ_{rot}, and G as global parameters. The calculations were carried out using a custom-built code[17] performing the χ^2 optimization. An example of the fit is shown in the top panel in Fig. 2 by black solid lines. The fit residuals are given in the middle and bottom panels for X and Y fluorescence polarizations, respectively. The quality of the fit for each measurement was found to be high. For the data in Fig. 2, the reduced χ^2 value was found to be $\chi^2/dof = 1.24$, where dof are the degrees of freedom, $dof = 26\,212$.

Note that formally good fit results for each individual measurement can suffer from possible systematic errors. In order to account for these, three independent measurements for each experimental geometry and each wavelength were performed. Differences between fit results for different measurements were found to be substantially larger than the fit errors for any individual measurement, indicating that systematic errors were significant in our experiment. Therefore, the fit parameters were averaged over three measurements. Their mean values and standard deviations are given in Tables I, II, and III.

Table I presents the isotropic (polarization-independent) parts of the fluorescence intensities at $t = 0$ at four excitation geometries. The values in Table I are normalized to the

TABLE II. Anisotropies for different effective excitation wavelengths λ. Mean values and standard deviations are estimated from three independent measurements for each wavelength. All values are given in percentage.

λ, nm	HH	VHX	VHY	RL	RR
268	13.15 ± 0.06	−18.7 ± 0.2	−1.5 ± 0.4	−6.8 ± 0.1	−6.27 ± 0.04
280	12.6 ± 0.3	−14.9 ± 1.41	−0.6 ± 1.3	−6.8 ± 0.4	−4.8 ± 0.2
286	13.1 ± 0.2	−17.2 ± 0.5	−2.2 ± 1.2	−6.9 ± 0.1	−5.3 ± 0.3
287	16.3 ± 0.1	−23.6 ± 1.1	2.2 ± 2.2	−9.7 ± 0.2	−8.6 ± 0.2
288	12.1 ± 0.2	−17.9 ± 2.4	−2.1 ± 0.3	−7.4 ± 0.4	−4.2 ± 0.2
289	15.2 ± 0.2	−23.7 ± 0.5	0.4 ± 1.3	−9.9 ± 0.3	−7.9 ± 0.6
293.33	16.0 ± 0.2	−20.2 ± 3.1	1.4 ± 3.3	−9.6 ± 0.6	−7.2 ± 0.8

TABLE III. Fluorescence lifetimes τ_f and rotational correlation times τ_{rot} for different effective excitation wavelengths λ.

λ, nm	268	280	268	287	288	289	293.33
τ_f, ps	3568 ± 8	3786 ± 18	3929 ± 23	3627 ± 6	3921 ± 16	3635 ± 12	3917 ± 27
τ_{rot}, ps	675 ± 20	805 ± 47	765 ± 61	725 ± 24	780 ± 9	641 ± 14	685 ± 33

intensity I_{HH} at each excitation wavelength. The normalized control sum $\Delta = (I_{HH} + I_{VH} - I_{RR} - I_{RL})/I_{HH}$ is given in the last column in Table I. According to the theoretical analysis,[17] this sum must be equal to zero. As can be seen from the last column in Table I the experimental data given in columns 2, 3, and 4 at each excitation wavelength satisfy the condition $\Delta = 0$ within error bars.

The two-photon excitation provides an important diagnostic tool for examining the excited state absorption properties which is the two-photon polarization ratio Ω defined as[28]

$$\Omega = \frac{I_c}{I_l}, \tag{3}$$

the ratio of two-photon absorptivities for circularly polarized versus linearly polarized light.

The two-photon polarization ratio Ω is given in the second column in Table I and is also presented in Fig. 3 as function of the effective excitation wavelength. Note that in our notation $\Omega = I_{RL}/I_{HH}$ because two excitation beams counter-propagated in our experiment (see also Herbrich *et al.*[18]).

Table II presents the fluorescence anisotropies $r(t)$ at $t = 0$ at seven effective excitation wavelengths. The number of anisotropies in columns 2–6 in Table II is larger than the number of experimental geometries used, because two independent anisotropies are introduced for the VH geometry, as mentioned above.

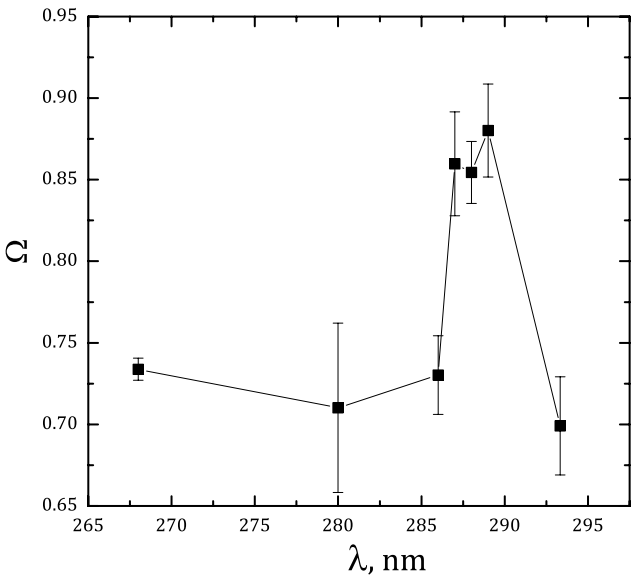

FIG. 3. Spectral dependence of the two-photon polarization ratio $\Omega = I_{\text{RL}}/I_{\text{HH}}$. Error-bars show the estimated standard deviations from three measurements.

The fluorescence lifetimes τ_f and rotational correlation times τ_{rot} are presented in Table III.

IV. DATA ANALYSIS AND DISCUSSION

A. Two-photon polarization ratio Ω

According to the theory,[1,32] the allowed range of the Ω-parameter in Eq. (3) is $0 \leqslant \Omega \leqslant 3/2$, where the maximal value is reached, for instance, when the excited state belongs to a non-totally symmetric representation. If the exited state belongs to the totally symmetric representation Ω may have any value within this range. In case of indole, both ^1L_a and ^1L_b excited states belong to the totally symmetric representation A'. As known,[28] the Ω-parameter values for these two states are significantly different. For the ^1L_b state Ω is about 1.4, close to the theoretical maximum, while for the ^1L_a state it is significantly lower, $\Omega \sim 0.5$–0.7.[28] Therefore, Ω is often used as a sensitive tool indicating the transition nature (^1L_a, ^1L_b, or mixed). However, sometimes this criterion can lead to a false assignment as the ^1L_b and ^1L_a states can interact with each other. As shown by Fender, Sammeth, and Callis[24] and by Küpper *et al.*[33] several ^1L_b vibronic bands at ~ 400 cm^{-1} (in vacuum) bear the ^1L_a character due to the Herzberg-Teller coupling in the vicinity of the conical intersection with the upper ^1L_a state.[34]

Our experimental result given in Fig. 3 demonstrates a relatively small mean value of $\Omega \approx 0.72$ with a statistically significant increase to $\Omega \approx 0.85$ at the 287–289 nm spectral range. This observation suggests that the two-photon excitation is dominated by the ^1L_a character with an admixture of the ^1L_b 0-0 band at about 288 nm. This conclusion is in a good agreement with the result reported by Rehms and Callis.[28] Note that due to solvent effects, the position of the ^1L_b 0-0 band at 288 nm (4.3 eV) in Fig. 3 is somehow red-shifted from the ^1L_b origin in vacuum.

Significant lowering of the Ω-value at the red edge indicates the solvent-induced state inversion under the condition of our experiment where ^1L_a becomes the lowest excited state. This suggestion can be supported by a quantitative criterion developed by Catalán and Diáz[30] based on the solvent polarity-polarizability scale SPP introduced by Catalán *et al.*[35] This scale is based on the solvatochromic shifts undergone by two reference solutes: 2-(dimethylamino)-7-nitrofluorene (DMANF) and 2-fluoro-7-nitrofluorene (FNF) and quantifies non-specific solvent-solute interactions. According to Catalán and Diáz,[30] the relationship of the position of the maxima in the fluorescence emission spectrum ν_{em} versus SPP splits into two distinct linear dependencies showing that the polar solvent leads to ^1L_a and ^1L_b reversal in indole at SPP $\gtrsim 0.8$.

As for propylene glycol SPP is equal to 0.87,[36] the lowest excited state is expected to be ^1L_a in perfect agreement with our findings. A similar behavior of Ω was observed by Rehms and Callis[28] for indole dissolved in butanol, also in agreement with the Catalán and Diáz[30] criterion because for butanol SPP = 0.84.

B. Two-photon molecular parameters $M_K(R, R')$ and the excitation tensor $S_{R\gamma}$

As already stated in the Introduction, the polarized fluorescence intensity in TPEF experiments for any experimental geometry depends on a number of time-dependent molecular parameters which contain all information on the two-photon excitation step and the subsequent evolution of the molecular excited state. In this paper, we used the set of molecular parameters $M_K(R, R', t)$ (M-parameters) based on the irreducible representation of the transition tensors,[15] where the parameter rank K is limited to 0, 2 and the arguments R, R' are limited to 0, 1, and 2, where $|R - R'| \le K$. At $t = 0$, these parameters can be presented as linear combinations of the McClain's molecular parameters $\hat{Q}_i$ based on the Cartesian tensor representation.[10,11]

Three zero-rank M-parameters describe the two-photon absorbance related to the isotropic part of the fluorescence and four second-rank M-parameters are responsible for fluorescence anisotropy. Note that the zeroth-rank parameters are positive by definition.[15] Moreover, the parameters with $R(R') = 1$ can be determined only in two-color experiments. An advantage of the irreducible representation is that it allows to recognize the identically zero M-parameters from the molecular point group symmetry.[13,15]

The general expression describing the 2C2P excited fluorescence intensity in terms of the molecular parameters derived in our previous paper (Eq. (1) and Table I in Ref. 17) was used for the determination of the M-parameters from experimental data. Note that under the conditions of this experiment the RR and RL rows in Table I in Ref. 17 were exchanged because, in the present work, the excitation beams propagated in opposite directions, while in Ref. 17 they propagated in the same direction.

Four fluorescence intensities: I_{HH}, I_{VH}, I_{RR}, and I_{RL} provide an over-determined linear system for determination of three zero-rank molecular parameters $M_0(R, R)$ with $R = 0, 1$, and 2. Accordingly, five anisotropy values in Table II, multiplied each by respective intensities, provide a linear system for determination of four remaining second rank M-parameters. These over-determined systems were solved using a least-squares fit accounting for the estimated standard deviations of the experimental values. The best-fit M-parameters values at $t = 0$ are given in Table IV for each excitation wavelength. The parameters are normalized to the corresponding $M_0(0, 0)$ values.

The set of M-parameters at $t = 0$ in Table IV together with the lifetimes τ_f and rotation correlation times τ_{rot} in Table III contains complete dynamical information which can be obtained from TPEF experiment.

According to the theory,[15] the M-parameters at $t = 0$ are related to the components of the two-photon excitation tensor

TABLE IV. Best-fit M-parameters normalized by $M_0(0, 0)$ for different effective excitation wavelengths λ.

λ, nm	$M_0(1, 1)$	$M_0(2, 2)$	$M_2(1, 1)$	$M_2(0, 2)$	$M_2(1, 2)$	$M_2(2, 2)$
268	−0.09	1.09	−0.01	0.45	0.11	0.50
280	−0.05	1.03	0.05	0.42	0.08	0.44
286	0.06	1.07	−0.06	0.44	0.13	0.46
287	0.02	1.43	−0.13	0.62	0.16	0.83
288	0.03	1.48	0.03	0.44	0.15	0.67
289	−0.03	1.52	−0.11	0.57	0.19	0.87
293.33	0.03	0.97	−0.02	0.54	0.09	0.56

$S_{R\gamma}$ and the fluorescence transition dipole moment $\mathbf{F}$ via the relation

$$M_K(R, R') = -\sqrt{3}([\mathbf{F}^* \otimes \mathbf{F}]_K \cdot [\mathbf{S}^*_{R'} \otimes \mathbf{S}_R]^*_K), \tag{4}$$

where the symbol ⊗ denotes the irreducible tensor product and the symbol (·) denotes the irreducible scalar product. The spherical components of the two-photon excitation tensor are given by[15]

$$S_{R\gamma} = \sum_{q_1 q_2, i} C^{R\gamma}_{1q_1 1q_2} \langle e|\hat{d}_{q_2}|i\rangle \langle i|\hat{d}_{q_1}|g\rangle \times \left(\frac{1}{E_i - E_g - \hbar\omega_1} + \frac{(-1)^R}{E_i - E_g - \hbar\omega_2}\right), \tag{5}$$

where summation is performed over all virtual intermediate states (i) including the ground state g and the final excited state e. E_i and E_g in Eq. (5) are intermediate and ground state energies, respectively, ω_1 and ω_2 are the frequencies of the first and the second photon, respectively, the indices $q_1, q_2 = -1, 0, 1$ are the transition dipole $\hat{\mathbf{d}}$ spherical components, and the term $C^{R\gamma}_{1q_1 1q_2}$ is a Clebsch–Gordan coefficient.[37]

As both excited states ^1L_b and ^1L_a belong to the same A' representation as the ground state, corresponding fluorescence dipole moments must be parallel to the molecular plane. According to Eq. (4), two-photon excitation tensor components can be defined with respect to the fluorescence dipole direction which will be set as molecular x axis. Following the usual definition,[38] we set the molecular z axis perpendicular to the molecular plane. Then the components of the two-photon excitation tensor which can differ from zero are as follows: S_{00}, S_{10}, S_{20}, and S_{22}. The relationship between the spherical and Cartesian components of the two-photon excitation tensor can be presented as (see, e.g., Ref. 37)

$$S_{00} = -\frac{1}{\sqrt{3}} Tr\mathbf{S} = -\frac{1}{\sqrt{3}}(S_{xx} + S_{yy} + S_{zz}), \tag{6}$$

$$S_{10} = \frac{i}{\sqrt{2}}(S_{xy} - S_{yx}), \tag{7}$$

$$S_{20} = \frac{1}{\sqrt{6}}(2S_{zz} - S_{xx} - S_{yy}), \tag{8}$$

$$S_{2\pm2} = \frac{1}{2}(S_{xx} - S_{yy}) \pm \frac{i}{2}(S_{xy} + S_{yx}). \tag{9}$$

According to Eqs. (6)–(9), the component S_{00} is real and proportional to the trace of the tensor $\mathbf{S}$, S_{20} is also real and represents the quadruple component of the tensor $\mathbf{S}$ describing the alignment of the tensor along the molecular z axis, S_{22} can

have complex value (in mathematical sense) and describes the anisotropy of the two-photon excitation in the xy molecular plane, and S_{10} is pure imaginary and describes the asymmetry of the tensor **S** in the xy plane. These conditions lower the number of independent parameters to five.

For inferring these parameters from nine non-linear equations (four for intensities and five for anisotropies), the maximum likelihood method was used based on the weighted least squares residuals. The weighting took into account unknown systematic errors and employs the estimated standard deviations shown in Tables I and II. This approach implicitly assumed that these systematic errors are Gaussian. The estimation of the fit parameter uncertainties and the likelihood calibration were performed numerically using the Markov chain Monte-Carlo (MCMC) sampling in the parameter space. The affine MCMC procedure[39] implemented in the freely available `python` package `emcee`[40] was employed. The two-photon excitation tensor components $S_{R\gamma}$ obtained in this way and normalized by the component S_{00} are given in Fig. 4. Error bars in Fig. 4 correspond to 90% uncertainties inferred from the MCMC marginal posterior distributions of model parameters.[41] A similar procedure can readily be used for the characterization of error bars of the M-parameters in Table IV.

As can be seen from Fig. 4, the main contribution to the signal is given by the two-photon excitation tensor components $Im\,S_{22}$ and S_{20}, while the contribution from the S_{10} and $Re\,S_{22}$ components are small. Considering the ratio S_{20}/S_{00} one can conclude that the out-of-plane component of the two-photon tensor is small. As can be easily seen from Eqs. (6) and (8), for pure planar two-photon tensor, this ratio is equal to $1/\sqrt{2} \approx 0.71$ which is close to the experimental values shown in Fig. 4. For all excitation wavelengths in Fig. 4, the component S_{zz} was found to be less than 4% of the **S**-tensor trace.

Also, as the S_{10} component in Fig. 4 is small, the tensor **S** is almost symmetric in the xy plane. Note that the signs

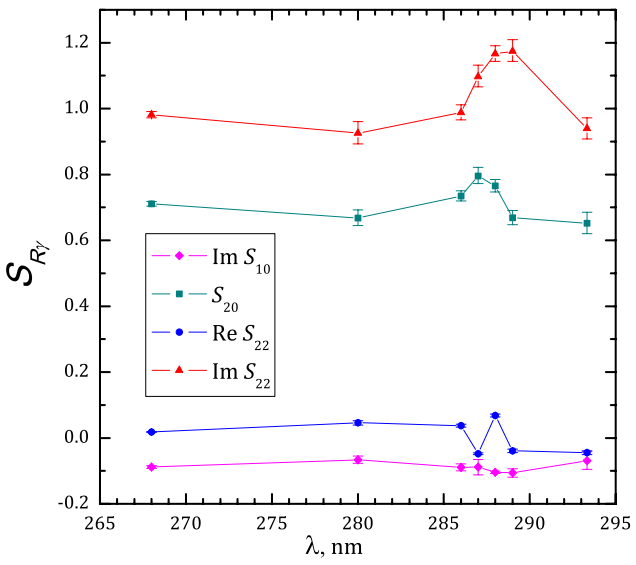

FIG. 4. Irreducible components of the two-photon excitation tensor $S_{R\gamma}$ as function of the excitation wavelength. The errors given are 90% credible intervals estimated via our MCMC simulations.

of the S_{10} and $Im\,S_{22}$ components cannot be determined from experiment, while their relative phase is fixed. This is because the expression used are invariant under the rotation of the coordinate system by the angle π over x axis. (The "up" and "down" directions of z axis are equivalent for a given x axis direction.) Here, we selected $Im\,S_{22} > 0$.

The analysis of the S_{22} component in Eq. (9) allows to determine the direction of the principal tensor axes and the in-plane tensor shape (elongation). Transformation of the irreducible tensor component S_{22} to the principal frame under rotation about the molecular z axis is given by $S'_{22} = \hat{R}_z(\phi)S_{22} = e^{-2i\phi}S_{22} = e^{i[arg(S_{22})-2\phi]}|S_{22}|$, where $\hat{R}_z(\phi)$ is a rotation operator and the superscript index ($'$) denotes the principal tensor frame. Having in mind that the tensor principal frame is characterized by the zero value of the symmetrized off-diagonal tensor component $S'_{xy} + S'_{yx} = 0$ and using Eq. (9), it is easy to see that $\phi = arg(S_{22})/2 \approx \pm\pi/4$, where the ($\pm$) sign is due to the ambiguity of the sign of $arg(S_{22})$ mentioned above. Thus, the long principal two-photon tensor axis is directed about $\pm\pi/4$ in the molecular frame with respect to the fluorescence dipole direction. The second solution: $\phi = arg(S_{22})/2 + \pi/2 \approx 3\pi/4$, or $\pi/4$ is related to the position of the second principal axis.

The component modulus in the principal frame is given by $|S'_{22}| = |S'_{xx} - S'_{yy}|/2$ and defines the tensor elongation. According to Eqs. (6) and (9), the ratio $|S'_{22}/S'_{00}|$ is equal to $\sqrt{3}/2 \approx 0.87$ if the off-plane component S_{zz} can be neglected and one of the in-plane components (S'_{xx}, or S'_{yy}) dominates. As shown in Fig. 4, the experimental value of the ratio varies in the range 0.9–1.2 which indicates that although the S'_{xx} component dominates, the contribution from the other component, S'_{yy} cannot be neglected. The analysis showed that the S'_{yy}/S'_{xx} ratio is negative and ranges from −4% to −6% for the ^1L_a state at 268–285 nm and from −10% to −16% for the ^1L_b state at 287–289 nm.

The determined **S**-tensor components can be visualized by plotting the two-photon transition tensor shape[29] which is the polar plot in the molecular frame where the radius r is proportional to the absorptivity of two photons both linearly polarized in the direction specified by the polar angle φ. A cut of the **S**-tensor shapes by the molecular plane is given in Fig. 5 for all effective excitation wavelengths used in our experiment with respect to the fluorescence dipole moment direction indicated by the solid line with two arrows. Each plot is normalized to unity in the direction of the maximum absorption.

As can be seen in Fig. 5, the plots related to different wavelengths are very similar to each other and do not show the peculiar structure as in Figs. 3 and 4 which is mainly because the structure manifests itself when circular polarized light is involved. According to the previous discussion, the lowest (and, therefore, fluorescent) state in the condition of our experiment is ^1L_a. The transition dipole moment direction of the ^1L_a state is not known in great detail; however, both experimental[21] and theoretical[42] considerations suggest that it is located at −46° with respect to the molecular long axis. The direction of +46° from the fluorescence dipole is shown by the dashed line with arrows in Fig. 5. The figure demonstrates remarkable alignment of the ^1L_a two-

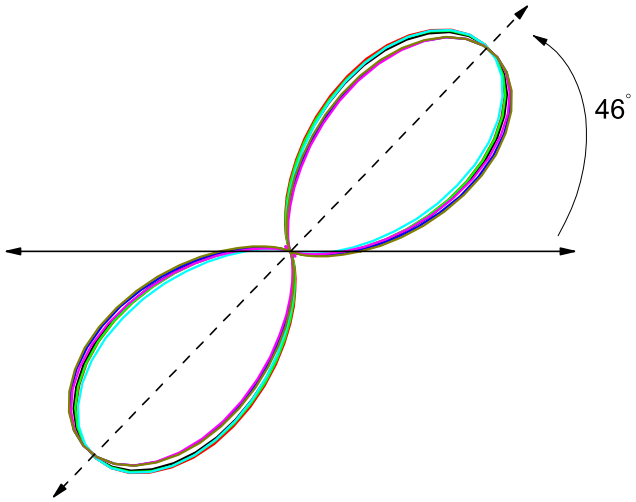

FIG. 5. Polar plot of the shapes of the two-photon tensors **S** for 7 excitation wavelengths. The solid line with arrows shows the direction of the fluorescence dipole. Dashed line at +46° from the fluorescence dipole indicates the estimated position of the molecular long axis.

photon tensor shape along the indole long axis. This result is in perfect agreement with the analysis given by Callis[29] who theoretically reconstructed the two-photon excitation tensors for ^1L_a and ^1L_b states. However, the analysis of the experimental data reported by Lakowicz *et al.*[43] has led to about 15° inclination of the two-photon tensor principal axis from the indole long axis.[29] We do not know the reason for this disagreement.

As already mentioned, only the absolute value of the angle between the fluorescence dipole and the long principal two-photon tensor axis can be determined from experiment. Therefore, the position of the two-photon tensor long principle axis can be formally set either parallel to the molecular long axis, or perpendicular to it. However, the latter possibility is strongly disfavored by calculations.[29] Also, the analysis has shown that there are two different solutions for the **S**-tensor components for the same M-parameters because the M-parameters remain the same under exchange of the S_{yy} and S_{zz} two-photon Cartesian tensor components. However, the second solution resulting in high S_{zz} and small S_{yy} components looks unrealistic as almost all theoretical and experimental studies done before resumed in predominately in-plane position of the transition dipoles for several first indole excited states.

C. Lifetime τ_f and correlation time τ_{rot}

The lifetime τ_f and rotation correlation time τ_{rot} experimentally determined at seven effective excitation wavelengths in the region 268–293.33 nm are given in Table III. As seen, the excited state lifetimes are in the range $\tau_f \approx 3.5 - 3.9$ ns and the rotational correlation times are in the range $\tau_{rot} \approx 0.6 - 0.8$ ns. Both lifetimes have practically no systematic wavelength dependence which is likely due to fast nonradiative intermolecular relaxation prior the fluorescence when the fluorescence does not rely on excitation history and occurs from the lowest excited state vibrational level. Assuming that these characteristic times has no, or negligible, dependence on the excitation wavelength we calculated their weighted average values as: $\tau_f = 3.83 \pm 0.14$ ns and $\tau_{rot} = 0.74 \pm 0.06$ ns.

V. CONCLUSIONS

We present the results of the complete polarization experiment in indole dissolved in propylene glycol using the 2C2P TPEF experimental method at seven effective excitation wavelengths in the 268–293.33 nm spectral region. Excitation with femtosecond laser pulses has allowed us to track the fluorescence temporal dependence with sub-nanosecond resolution and obtain from experiment the fluorescence lifetime and rotational correlation time. As shown, the main excitation pathway was the transition to the ^1L_a state which becomes the lowest in energy due to interaction with the polar solvent. The ^1L_b origin manifests itself at about 288 nm by a hump in the two-photon polarization ratio Ω spectral dependence. Combining different geometries, we were able to infer from experiment all components of the two-photon excitation tensor **S**. As found, the tensor **S** is almost symmetric and planar in the molecular plane for all excitation wavelengths, the off-plane tensor component S_{zz} is less than 4% of the in-plane components. Also, the long principal two-photon tensor axis was found to be directed about $\pm\pi/4$ with respect to the fluorescence dipole direction in the molecular frame and parallel/perpendicular to the molecular long axis. Moreover, the ratio of the parallel/perpendicular tensor components S_{yy}/S_{xx} was found to be negative and ranges from −4% to −6% at 268–285 nm where the absorption to ^1L_a dominates and from −10% to −16% at the 287–289 nm spectral range, where the contribution from ^1L_b origin is significant. The lifetime τ_f and the rotation correlation time τ_{rot} were found to have practically no dependence on the effective excitation wavelength.

ACKNOWLEDGMENTS

The authors thank Dr. Christof Maul for fruitful discussions. P.S.S., A.G.S., and O.S.V. are grateful to the Russian Science Foundation for financial support, Project No. 14-13-00266.

[1]*Topics in Fluorescence Spectroscopy. V.5 Nonlinear and Two-Photon-Induced Fluorescence*, edited by J. R. Lakowicz (Plenum Press, New York, 1997).
[2]W. M. McClain, Acc. Chem. Res. **7**, 129 (1974).
[3]W. Denk, J. H. Strickler, and W. W. Webb, Science **248**(4951), 73 (1990).
[4]I. Gryczynski, H. Malak, and J. R. Lakowicz, Biospectroscopy **3**, 97 (1997).
[5]J. R. Lakowicz, I. Gryczynski, H. Malak, and Z. Gryczynski, Photochem. Photobiol. **64**, 632 (1996).
[6]J. R. Lakowicz, I. Gryczynski, H. Malak, and Z. Gryczynski, J. Phys. Chem. **100**, 19406 (1996).
[7]J. Palero, W. Garcia, and C. Saloma, Opt. Commun. **211**, 65 (2002).
[8]S. Quentmeier, S. Denicke, J.-E. Ehlers, R. A. Niesner, and K.-H. Gericke, J. Phys. Chem. B **112**, 5768 (2008).
[9]S. Denicke, S. Quentmeier, J.-E. Ehlers, and K.-H. Gericke, Phys. Scr. **80**, 048105 (2009).
[10]W. M. McClain, J. Chem. Phys. **57**, 2264 (1972).
[11]W. M. McClain, J. Chem. Phys. **58**, 324 (1973).
[12]F. Metz, W. E. Howard, L. Wunsch, N. J. Neusser, and E. W. Schlag, Proc. R. Soc. London, Ser. A **363**, 381 (1978).

[13]V. A. Gaisenok, J. Appl. Spectrosc. **49**, 1087 (1988).
[14]C. Wan and C. K. Johnson, Chem. Phys. **179**, 513 (1994).
[15]P. S. Shternin, K.-H. Gericke, and O. S. Vasyutinskii, Mol. Phys. **108**, 813 (2009).
[16]L. Ryderfors, E. Mukhtar, and L. B.-Å. Johansson, J. Phys. Chem. A **112**, 5794 (2008).
[17]S. Denicke, K.-H. Gericke, A. G. Smolin, P. Shternin, and O. Vasyutinskii, J. Phys. Chem. A **114**, 9681 (2010).
[18]S. Herbrich, K.-H. Gericke, A. G. Smolin, and O. S. Vasyutinskii, J. Phys. Chem. A **118**, 5248 (2014).
[19]A. P. Demchenko, *Ultraviolet Spectroscopy of Proteins* (Springer-Verlag, Berlin, 1986).
[20]J. R. Platt, J. Chem. Phys **17**, 484 (1949).
[21]B. Albinsson and B. Nordén, J. Phys. Chem. **96**, 6204 (1992).
[22]J. W. Hager and S. C. Wallace, J. Phys. Chem. **87**, 2121 (1983).
[23]E. H. Strickland, J. Horwitz, and C. Billups, Biochemistry **25**, 4914 (1970).
[24]B. J. Fender, D. M. Sammeth, and P. R. Callis, Chem. Phys. Lett. **239**, 31 (1995).
[25]V. A. Povedailo and D. L. Yakovlev, J. Appl. Spectrosc. **75**, 336 (2008).
[26]H. Lami and N. Glasser, J. Chem. Phys. **84**, 597 (1986).
[27]C. Kang, T. M. Korter, and D. W. Pratt, J. Chem. Phys. **122**, 174301 (2005).
[28]A. A. Rehms and P. R. Callis, Chem. Phys. Lett. **140**, 83 (1987).
[29]P. R. Callis, J. Chem. Phys. **99**, 27 (1993).
[30]J. Catalán and C. Diáz, Chem. Phys. Lett. **368**, 717 (2003).
[31]W. T. Huntress, Jr., J. Chem. Phys. **48**, 3524 (1968).
[32]R. P. Drucker and W. M. McClain, J. Chem. Phys. **61**, 2609 (1974).
[33]J. Küpper, D. W. Pratt, W. Leo Meerts, C. Brand, J. Tatchen, and M. Schmitt, Phys. Chem. Chem. Phys. **12**, 4980 (2010).
[34]G. N. Ten, A. A. Yakovleva, M. K. Berezin, and V. I. Baranov, Opt. Spectrosc. **114**, 590 (2013).
[35]J. Catalán, V. López, P. Pérez, R. Matin-Villamil, and J. G. Rodriguez, Liebigs Ann. **1995**, 241.
[36]J. Catálan, J. Phys. Chem. B **113**, 5951–5960 (2009).
[37]D. A. Varshalovich, A. N. Moskalev, and V. K. Khersonskii, *Quantum Theory of Angular Momentum* (World Scientific, Singapore, 1988).
[38]P. R. Callis, Annu. Rev. Phys. Chem. **48**, 271 (1997).
[39]J. Goodman and J. Weare, Commun. Appl. Math. Comput. Sci. **5**, 65 (2010).
[40]D. Foreman-Mackey, D. W. Hogg, D. Lang, and J. Goodman, Publ. Astron. Soc. Pac. **125**, 306 (2013).
[41]A. Gelman, J. B. Carlin, H. S. Stern, and D. B. Rubin, *Bayesian Data Analysis* (Chapman and Hall/CRC, Boca Raton, 2004).
[42]C. Brand, J. Küpper, D. W. Pratt, W. Leo Meerts, D. Krügler, J. Tatchen, and M. Schmitt, Phys. Chem. Chem. Phys. **12**, 4968 (2010).
[43]J. R. Lakowicz, I. Gryczynski, E. Danielsen, and J. Frisoli, Chem. Phys. Lett. **194**, 282 (1992).